

COMPARISON OF THE PERFORMANCE OF FOUR EULERIAN NETWORK FLOW MODELS FOR STRATEGIC AIR TRAFFIC MANAGEMENT

DENGFENG SUN

604 Davis Hall, University of California
Berkeley, CA 94720-1710, USA

ISSAM S. STRUB

604 Davis Hall, University of California
Berkeley, CA 94720-1710, USA

ALEXANDRE M. BAYEN

711 Davis Hall, University of California
Berkeley, CA 94720-1710, USA

ABSTRACT. Four Eulerian network models are implemented to model high altitude air traffic flow. Three of the models use the framework of discrete time dynamical systems, while the fourth consists of a network of partial differential equations. The construction of these models is done using one year of air traffic data. The four models are applied to high altitude traffic for six *Air Route Traffic Control Centers* in the *National Airspace System* and surrounding airspace. Simulations are carried out for a full day of data for each of the models, to assess their predictive capabilities. The models' predictions are compared to the recorded flight data. Several error metrics are used to characterize the relative accuracy of the models. The efficiency of the respective models is also compared in terms of computational time and memory requirements for the scenarios of interest. Control strategies are designed and implemented on similar benchmark scenarios for two of the models. They use techniques such as adjoint-based optimization, as well as mixed integer linear programming. A discussion of the four models' structural differences explains why one model may outperform another.

1. Introduction. With the uninterrupted growth of air traffic over the last few decades, strategic *Traffic Flow Management* (TFM) has become a very important issue in the study of the *National Airspace System* (NAS), which is a complex physical system consisting of aircraft, control facilities, procedures, navigation and surveillance equipment, analysis equipment, decision support tools, and controllers who operate the system [4]. One of the key elements in TFM is the *Air Traffic Control* (ATC) system, which helps Air Traffic Controllers manage the increasing complexity of traffic flow in the en route airspace. ATC is operated at the sector level, where a sector is a small portion of the airspace controlled by a single human Air Traffic Controller [25]. TFM typically deals with traffic at the *Air Route Traffic*

2000 *Mathematics Subject Classification.* Primary: 90B10, 90B20; Secondary: 90C11, 76B75.

Key words and phrases. Network flow model; air traffic flow management.

This work was supported by NASA under Task Order TO.048.0.BS.AF.

Control Center (ARTCC) level, i.e. 10 to 20 sectors. TFM problems include maintaining the aircraft count in each sector below a legal threshold in order to ensure the safety of the flights, as well as to ease the human ATC workload [10]. This task is quite cumbersome; furthermore, extensive traffic forecast simulations (including all airborne aircraft) are computationally too expensive to include systematic investigations of traffic patterns that lead to sector overload [4].

As a result, a new class of traffic flow models has emerged from recent studies: *Eulerian* models, which aim at studying the design of optimized flows in the NAS. Eulerian models [4, 23, 24, 34] are control-volume based, which means that they rely on conservation equations. This is in contrast to *Lagrangian* models, which are trajectory-based and take into account individual aircraft trajectories [3]. Eulerian models have two main advantages over Lagrangian models. (i) Their computational complexity depends only on the size of the physical problem of interest, rather than the number of aircraft. (ii) Their mathematical structure enables the use of standard methods to analyze them, such as control theory or optimization.

The field of Eulerian network modeling for the NAS is strongly inspired by hydrodynamic theory for highway traffic flow (see in particular the work of Lighthill, Whitham and Richards [20, 27], and its discrete counterparts in the highway traffic literature [8, 9]). This framework is sometimes referred to as the *LWR theory* [33], and was introduced in [23] in the context of air traffic. This work was subsequently extended by the same authors, including a tessellation model which partitions the NAS into two dimensional cells and studies traffic flows through this cellular network [24]. Aggregate models were later adapted to include a stochastic framework [30, 32], in which data aggregation procedures enable predictions of flows in the expected sense. Adjoint-based techniques [4] were subsequently developed for a fully continuous NAS model (i.e. using partial differential equations), which was also used for modeling behavior of single agents (airlines) in the NAS [26]. In order to alleviate the problems due to network splits inherent to most of the aforementioned models, a multicommodity *Large-capacity Cell Transmission Model* (CTM(L)) based on network flow techniques [14] was finally proposed [28, 34] and successfully implemented.

The field of control and optimization of physical networks is a very wide area, for which numerous research efforts have led to the development of several methods to deal with networks of distributed parameter systems. Several of them can be mentioned here, because of their relevance to our work. Networks of interconnected roads are modeled and studied in the recent book of Garavello and Piccoli [11] and can be used for the study of highway traffic flow. A variety of techniques exist for optimization of physical networks. Frequency domain approaches have been used by Litrico et al. in the context of canal network control for the Saint-Venant equations [21] and provide useful control techniques when underlying equations of flows are linear. Linear quadratic optimal control theory was applied by Malaterre for the automatic control of two different eight-pool irrigation canals [22]. Several approaches have been developed to deal with nonlinear phenomenon present in physical networks. A nonlinear output feedback method was studied in [2] for a compartmental network flow system. From a macroscopic point of view, Haut et al. modeled the junctions in a road network, which presents physically acceptable solutions and is able to represent the capacity drop phenomenon in highway systems [13]. Methods based on Lyapunov functions were presented by Coron et al. for a hydraulic application, namely the level and flow regulation in a horizontal

open channel [7]. A decentralized nonlinear control approach was used in [17] for fluid flow networks, where actuator valves and flow rate sensors are collocated in individual branches and do not exchange information. A similar model was used for optimal control of supply networks in [16].

In the present article, the control techniques used are driven by the mathematical features of the underlying flow models developed. We present four different aggregate Eulerian models of en route (high altitude) air traffic flow. We start with the large-capacity cell transmission model derived in earlier work [28, 34]. We present a modified version of the Menon model [23], adapted to fit a general network topology. We also present a new application of the Lax Wendroff scheme to a PDE model developed earlier in [4]. Finally, we implement the two-dimensional Menon model [24] at a NAS-wide level. We implement and compare predictive capabilities of the four models above on the same benchmark problem, for fairness of the comparison. Control strategies are designed and implemented on for the scenario of controlling sector counts for two of the models. This article is thus the first NAS-wide implementation of the four aforementioned models, and the first comparison of their respective performance on the same benchmark scenario.

We expect that this work will impact TFM research in the following areas: *(i)* automated bottleneck identification in the NAS; *(ii)* study of the uncertainty in en route demand and the volatility associated with seasonal patterns; *(iii)* NAS-wide characterization of delay and workload; *(iv)* design and implementation of new *Airspace Flow Programs* (AFP); *(v)* impact of weather on high altitude traffic flow.

This article is organized as follows. In the next section, the formulations of the four models are summarized. Section 3 assesses the predictive capabilities of each model through a careful validation against recorded *Aircraft Situation Display to Industry* (ASDI) and *Enhanced Traffic Management System* (ETMS) data. Section 4 illustrates the design of control strategies for the models. Section 5 compares the performance of the different models, in particular, accuracy of predictive capabilities, computational time, and memory requirements. A discussion follows which highlights the structural differences between the four models and explains why one model may outperform another. Finally, conclusions are presented in Section 6.

2. Models. This section presents a short summary of each of the four models used for this study. A detailed description of each model is available in the corresponding references.

2.1. The Large-capacity Cell Transmission Model (CTM(L)). The *Large-capacity Cell Transmission Model* (CTM(L)) is a new Eulerian traffic flow model developed in [34, 29]. It uses a graph-theoretic representation of traffic flow. Air traffic flow on this graph is modeled as a discrete time dynamical system evolving on a network. To formulate the model, the following assumptions are made:

1. Each link of the network is modeled as a directional edge.
2. All aircraft in a given link fly at an aggregate speed. This speed can be obtained by aggregating the speed (obtained from the ASDI/ETMS data) of all aircraft following this link.
3. The number of cells in one link is given by the number of steps of expected travel time. In this implementation, 1 minute is taken as a unit time step. For example, if it takes around 12 minutes for an aircraft to fly across a sector, following a particular link, then this link would be divided into 12 segments, called *cells*. The choice of the cell length (time discretization) is arbitrary. In

the model, a link indexed by i has m_i cells. As the time step decreases, the model becomes more accurate, but at the expense of increased computational complexity.

4. At the link level, only high altitude traffic (above 24,000 feet) is taken into account for the calculation of aircraft count. This choice is also arbitrary and can be adjusted to any user-defined level.
5. The control strategy (based on application of delays to aircraft) is mainly used as the controlled input to the model, which can be implemented in many forms: speed change, *vector for spacing* (VFS), *holding pattern* (HP), etc. It is applied in time increment corresponding to the unit time step.
6. The model is *deterministic*. No statistical factor, such as weather impact, is taken into consideration at this stage. Note that it could be added later using a stochastic framework [30, 31].
7. In this model, all states, inputs, and outputs, are integer valued. This might increase the complexity of computation or analysis, in particular, the computational complexity for optimization which is integer programming, but provides higher accuracy.

Under the assumption that air traffic flow can be accurately represented by an aggregated travel time, the behavior of aircraft flow on a single link can be modeled by a deterministic linear dynamical system with unit time delay, defined as follows [34]:

$$x_i(k+1) = A_i x_i(k) + B_i^f f_i(k) + B_i^u u_i(k) \quad (1)$$

$$y(k) = C_i x_i(k) \quad (2)$$

where $x_i(k) = [x_i^{m_i}(k), \dots, x_i^1(k)]^T$ is the state vector, whose elements represent the corresponding aircraft counts in each cell of link i at time step k , and m_i is the number of cells in the link. The forcing input, $f_i(k)$, is a scalar which denotes the entry count onto link i during a unit time interval from k to $k+1$, and the control input, $u_i(k)$ is an $m_i \times 1$ vector, representing holding pattern control. The output, $y(k)$, is the aircraft count in a user-specified set of cells at time step k . The nonzero elements of the $m_i \times 1$ vector C_i correspond to the cells in the user-specified set, and are equal to one. A_i is an $m_i \times m_i$ nilpotent matrix with 1's on its super-diagonal. $B_i^f = [0, \dots, 0, 1]^T$ is the forcing vector with m_i elements, and B_i^u is the $m_i \times m_i$ holding pattern matrix, in which all nonzero elements are 1 on the diagonal and -1 on the super-diagonal.

Because there is no interconnection between different links in one sector, it is straightforward to extend this modeling technique to set up a sector level model as follows. Suppose there are n links in a sector, then the state space equations for the model at the sector level can be described as:

$$x(k+1) = Ax(k) + B^f f(k) + B^u u(k) \quad (3)$$

$$y(k) = Cx(k) \quad (4)$$

where $x(k) = [x_n(k); \dots; x_1(k)]^T$ denotes the state, and $f(k) = [f_n(k); \dots; f_1(k)]^T$ is the forcing input vector (the entry count onto the sector). The control input vector $u(k) = [u_n(k); \dots; u_1(k)]^T$. The vector $y(k)$ represents the aircraft count in a user-specified set of cells at time step k . The matrices A , B^f , and B^u are block diagonal, with block elements associated with each link in the sector. For example, $A = \text{diag}(A_n, \dots, A_1)$ with A_i 's defined by Equations (1).

When an ARTCC level model is created, it is necessary to include *merge/diverge* nodes in the network [23, 30, 4, 32]. Merge nodes are straightforward: flows are

added as streams of aircraft merge. For diverge nodes, the corresponding routing choices must rely on knowledge of aircraft destination. Modeling the problem is proposed based on *a priori* knowledge of the destination of the aircraft (provided by ASDI/ETMS data): knowledge of each aircraft destination is available long before its departure, in the form of filed flight plans. One significant contribution of the CTM(L) is to incorporate this knowledge into the model, while previous Eulerian models do not [23, 24, 30, 31, 4], with use of the notion of multicommodity flow. More details are available in [34].

2.2. The Modified Menon Model (MMM). This section is based on the work presented in [23]. The model has been modified to fit the structure of the graph model that will be discussed in Section 2.5.

The original Menon model is an Eulerian traffic flow model in which the air traffic is spatially aggregated into control volumes, which are line elements [23]. It is based on the Daganzo *Cell Transmission Model* (CTM) [8, 9] in which the traffic flowing into a control volume changes the density of aircraft in the control volume and, hence, changes the outflow from the control volume. Several modifications of the original Menon model are made and outlined at the end of this subsection; we will thus refer to the improved version of the model as the *Modified Menon Model* (MMM). The model is also able to account for ATC actuation, and handle merging and diverging air traffic flows. The model consists of two parts, the one-dimensional control volume model and the merge and diverge routing structure.

The one-dimensional control volume model models air traffic flow as a network of inter-connected control cells through which the air traffic flows. Aircraft counts in the network can be described by the discrete-time difference equation:

$$x_j(i+1) = x_j(i) + \tau_j[y_{j-1}(i) - y_j(i)] \quad (5)$$

In the above equation, $x_j(i+1)$ is the aircraft count of control volume j at time $i+1$. The flow into j is $y_{j-1}(i)$ and $y_j(i)$ is equal to the flow out of j . The time step τ_j is computed by dividing the cell dimension, Ω_j , by the aircraft speed in the cell, v_j ($\tau_j = \Omega_j/v_j$). In other words, τ_j is the time an aircraft takes to travel through the cell.

The effects of delaying aircraft due to ATC actuation is accounted for by recirculating some of the air traffic flow in a control volume. The recirculated air traffic flow in control volume j is defined as u_j . The physical constraint on u_j is that at time i , it can not be greater than the existing flow in the cell or less than 0,

$$0 \leq \tau_j u_j(i) \leq x_j(i) \quad (6)$$

By including u_j and writing down the equation for y_j , the model can be written in the form of a linear, discrete-time dynamical system:

$$x_j(i+1) = a_j x_j(i) + \tau_j u_j(i) + \tau_j y_{j-1}(i) \quad (7)$$

$$y_j(i) = b_j x_j(i) - u_j(i) \quad (8)$$

The coefficients, a_j , b_j , and τ_j handle the conversion between the air traffic flow, y_j , and the aircraft count, x_j . In other words, at a given time step, a_j is the portion of aircraft remaining in the volume, and b_j is the portion of air traffic flow leaving the volume. As was noted earlier, τ_j is the length of time needed for the aircraft to travel the length of the control volume. The coefficients are defined in terms of Ω_j , the control volume length, and v_j , the aircraft speed.

$$a_j = (1 - v_j \tau_j / \Omega_j), \quad b_j = v_j / \Omega_j, \quad \tau_j = \Omega_j / v_j \quad (9)$$

The original Menon model assumes that velocity is constant within a given control volume. This means that a_j is always zero (see equation (13) in the original article [23]). That is, if there is no control from u_j , then all the aircraft in the volume travel to the subsequent volume on the next time step.

Intuitively, what is happening in equations (7) and (8) is that the aircraft count in a given control volume at time $i + 1$ depends on the number of aircraft in the volume at time i , the number of aircraft that flow into the volume, the number of aircraft that are recirculated and the number of aircraft that flow out of the volume. Over multiple time steps, aircraft will move through successive cells.

In a network of inter-connected control volumes, there may be points where air traffic coming from different directions merge into a single flow. This type of situation is referred to as a merge node. Furthermore, there may be points where the air traffic in one direction diverges into multiple flows. This type of situation is referred to as a diverge node. Because the nodes do not retain any aircraft, the conservation principle implies that for merge nodes, the resulting air traffic flow is the sum of all air traffic flows into that node. For example, if the air traffic flows q_{k-1} and q_{k-2} merge into q_k ,

$$q_k = q_{k-1} + q_{k-2} \quad (10)$$

Likewise, diverge nodes make use of the same conservation principle and the flow along a path from a diverge node is some proportion of the total flow coming into the diverge node. The proportion is defined as the divergence parameter, β , and is the ratio of aircraft travelling out of the diverge node along a given path over the aircraft travelling into the diverge node. In the following example, the air traffic flow diverges from the q_k to q_{k+1} and q_{k+2} ,

$$q_{k+1} = \beta q_k, \quad q_{k+2} = (1 - \beta) q_k \quad (11)$$

As mentioned earlier, since the MMM is implemented on a graph model of traffic flow constructed in the articles [28, 34] and discussed in Section 2.5, a number of modifications are made to improve the original Menon model described in the article [23].

1. The flights in the MMM are aggregated according to the links of the graph structure defined in our earlier work, and not the graph model presented in their original article [23]. This will ensure fairness of the comparison with the other models.
2. A link length (physical distance) is determined from flights in the data: flights in the data are aggregated according to the links in the graph. A link's entry and exit locations are determined by those flights' link entries and exits. The entry and exit locations are used in computing the link's length.
3. The MMM contains merge-diverge nodes. A merge-diverge node is one that has both merging and diverging flows at the same time. The original Menon model does not have such nodes.
4. A merge-diverge node can have n ($n \geq 2$) outflows, whose β values are determined from the data, whereas in the original Menon model n is limited to $n = 2$.

2.3. The PDE model. This section is based on work initiated in [4]. This model divides the airspace into line elements. These line elements are called paths and in practice often coincide with jetways. We represent a link on a path as a segment $[0, L]$ and we define $C(x, t)$ as the number of aircraft between distances 0 and x at time t . In particular, $C(0, t) = 0$, and $C(L, t)$ is the total number of aircraft in the path modeled by $[0, L]$ at time t . We make the additional assumption of a steady velocity profile $v(x) > 0$, which depicts the average velocity of aircraft flow at position x and time t . Applying the conservation of mass to a control volume comprised between positions x and $x + h$, and letting h tend to 0, one easily finds the following relation between the spatial and temporal derivatives of $C(x, t)$ [4]:

$$\begin{cases} \frac{\partial C(x,t)}{\partial t} + v(x)\frac{\partial C(x,t)}{\partial x} = q(t) & (x, t) \in (0, L) \times (0, T) \\ C(x, 0) = C_0(x) & x \in [0, L] \\ C(0, t) = 0 & t \in [0, T] \end{cases} \tag{12}$$

where $q(t)$ represents the inflow at the entrance of the link ($x = 0$). Alternatively, $q(t)$ can be defined in terms of the density as $q(t) = \rho(0, t)v(0)$.

We can define the density of aircraft as the weak derivative of $C(x, t)$ with respect to x : $\rho(x, t) = \frac{\partial C(x,t)}{\partial x}$. The aircraft density is a solution to the partial differential equation:

$$\begin{cases} \frac{\partial \rho(x,t)}{\partial t} + \frac{\partial(\rho(x,t)v(x,t))}{\partial x} = 0 & (x, t) \in (0, L) \times (0, T) \\ \rho(x, 0) = \rho_0(x) & x \in [0, L] \\ \rho(0, t) = \frac{q(t)}{v(0)} & t \in [0, T] \end{cases} \tag{13}$$

or in a nonconservative form:

$$\begin{cases} \frac{\partial \rho(x,t)}{\partial t} + v(x)\frac{\partial \rho(x,t)}{\partial x} + v'(x)\rho(x, t) = 0 & (x, t) \in (0, L) \times (0, T) \\ \rho(x, 0) = \rho_0(x) & x \in [0, L] \\ \rho(0, t) = \frac{q(t)}{v(0)} & t \in [0, T] \end{cases} \tag{14}$$

This is a linear advection equation with positive velocity $v(x)$ and a source term: $v'(x)\rho(x, t)$. Clearly, these two partial differential equations are equivalent and model the same physical phenomenon. In this article, we will use the latter for control, as it enables us to impose constraints in terms of aircraft density. We will use the former for simulation and comparison, because the aircraft count is more readily available from experimental data.

Now that the model has been defined on one link, we will extend it to a network. We consider a junction with m incoming links numbered from 1 to m and n outgoing links numbered from $m + 1$ to $m + n$; each link k is represented by an interval $[0, L_k]$ (Figure 1). One can see that any network is composed of a number of such junctions. We define an allocation matrix $M(t) = (m_{ij}(t))$ for $1 \leq i \leq m$, $m + 1 \leq j \leq m + n$, where $0 \leq m_{ij}(t) \leq 1$ denotes the proportion of aircraft from incoming link i going to the outgoing link j ; we also require $\sum_{j=m+1}^{m+n} m_{ij}(t) = 1$ for $1 \leq i \leq m$. The system of partial differential equations on the network can be written as:

$$\begin{cases} \frac{\partial \rho_k(x,t)}{\partial t} + v_k(x)\frac{\partial \rho_k(x,t)}{\partial x} + v'_k(x)\rho_k(x, t) = 0 & 1 \leq k \leq m + n, (x, t) \in (0, L_k) \times (0, T) \\ \rho_k(x, 0) = \rho_{0,k}(x) & x \in [0, L_k] \\ \rho_i(0, t) = \frac{q_i(t)}{v_i(0)} & 1 \leq i \leq m, t \in [0, T] \\ \rho_j(0, t) = \frac{\sum_{i=1}^m m_{ij}(t)\rho_i(L_i, t)v_i(L_i)}{v_j(0)} & m + 1 \leq j \leq m + n, t \in [0, T] \end{cases} \tag{15}$$

We will now show that on such a network, the preceding system of partial differential equations admits a unique solution hence that the problem is well-posed.

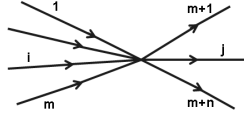


FIGURE 1. A junction with m incoming links ($1 \leq i \leq m$) and n outgoing links ($m + 1 \leq j \leq m + n$).

First we consider the case of a single link $[0, L]$. Since the velocity is always positive, a boundary condition shall be set on the left ($x = 0$) but not on the right ($x = L$). Using classical partial differential equations techniques, more precisely the theory of characteristics to compute the solution and prove the existence and energy methods for the uniqueness, it can be shown that the advection equation will have a unique solution on this interval (see for example [18] or [4] for a proof). On a network, this ensures the existence and uniqueness of a solution on the incoming links. For the outgoing links, we need to impose a boundary condition on the left, that is, immediately after the junction. This is done using the coefficients of the allocation matrix. Indeed for the j -th outgoing link, the density at the origin will be related to the densities at the right extremity of the incoming links by:

$$\rho_j(0, t) = \frac{\sum_{i=1}^m m_{ij}(t) \rho_i(L_i, t) v_i(L_i)}{v_j(0)}$$

Now the advection equation on each outgoing link has a unique solution, thus uniquely defining a density on both the incoming and outgoing links. Therefore, the problem for any network, which is made of several such junctions, is well-posed.

We apply the Lax-Wendroff scheme to the preceding partial differential equation. We use a discrete grid on the domain $[0, L] \times [0, T]$:

$$x_a = \frac{aL}{M}, \quad 0 \leq a \leq M \quad \text{and} \quad t_b = \frac{bT}{N}, \quad 0 \leq b \leq N$$

and

$$\Delta x = \frac{L}{M}, \quad \Delta t = \frac{T}{N}$$

The Lax-Wendroff scheme (see [19]) is based on the second order Taylor series expansion of $C(x, t)$

$$C(x, t_{b+1}) = C(x, t_b) + (\Delta t) C_t(x, t_b) + \frac{1}{2} (\Delta t)^2 C_{tt}(x, t_b) + \dots$$

Given that $C(x, t)$ is a solution of the partial differential equation above, we have:

$$C_t(x, t) = -v(x) C_x(x, t) - v'(x) C(x, t)$$

$$C_{tt}(x, t) = -v(x) C_{xt}(x, t) - v'(x) C_t(x, t)$$

If we differentiate the expression of $C_t(x, t)$ with respect to x , we obtain: $C_{xt}(x, t) = -v(x) C_{xx}(x, t) - v''(x) C(x, t) - 2v'(x) C_x(x, t)$ which yields:

$$\begin{aligned} C_{tt}(x, t) = & v^2(x) C_{xx}(x, t) + 3v(x) v'(x) C_x(x, t) \\ & + (v(x) v''(x) + (v'(x))^2) C(x, t) \end{aligned}$$

Using the preceding expressions of $C_t(x, t)$ and $C_{tt}(x, t)$ in the Taylor series expansion, we find:

$$\begin{aligned} C(x, t_{b+1}) &= C(x, t_b) - (\Delta t)v(x)C_x(x, t_b) - (\Delta t)v'(x)C(x, t_b) \\ &\quad + \frac{1}{2}(\Delta t)^2(v^2(x)C_{xx}(x, t_b) + 3v(x)v'(x)C_x(x, t_b) \\ &\quad + (v(x)v''(x) + (v'(x))^2)C(x, t_b)) + \dots \end{aligned}$$

Then we replace the spatial derivatives by central finite difference approximations:

$$\begin{aligned} C_x(x, t) &\leftrightarrow \frac{C^{a+1,b} - C^{a-1,b}}{2\Delta x} \\ C_{xx}(x, t) &\leftrightarrow \frac{C^{a-1,b} - 2C^{a,b} + C^{a+1,b}}{(\Delta x)^2} \end{aligned}$$

We eventually obtain the Lax-Wendroff scheme:

$$\begin{aligned} C^{a,b+1} &= \left(1 - (\Delta t)v'(x_a) + \frac{(\Delta t)^2}{2}(v(x_a)v''(x_a) + (v'(x_a))^2)\right) C^{a,b} \\ &\quad + \frac{\Delta t}{2\Delta x}v(x_a) \left(\frac{3}{2}(\Delta t)v'(x_a) - 1\right) (C^{a+1,b} - C^{a-1,b}) \\ &\quad + \frac{1}{2} \left(\frac{\Delta t}{\Delta x}\right)^2 v^2(x_a)(C^{a-1,b} - 2C^{a,b} + C^{a+1,b}) \end{aligned}$$

The initial condition implies:

$$C^{a,0} = \frac{1}{2\Delta x} \int_{x_{a-1}}^{x_{a+1}} C_0(x) dx \text{ for } 0 \leq a \leq M$$

The boundary conditions are implemented using 2 ghost-cells on the left and right of the spatial domain. Given that the velocity is always positive, the boundary conditions can only be prescribed on the left; we use zero-order extrapolation for the right boundary condition:

$$C^{-1,b} = \frac{1}{\Delta t} \int_{t_b}^{t_{b+1}} \frac{q(t)}{v(0)} dt \text{ and } C^{M+1,b} = C^{M,b} \text{ for } 1 \leq b \leq N$$

Finally, when choosing the space and time steps, the *Courant-Friedrichs-Lewy* (CFL) condition has to be verified:

$$\left| \frac{v(x)\Delta t}{\Delta x} \right| \leq 1 \text{ for } x \in [0, L]$$

where $\left| \frac{v(x)\Delta t}{\Delta x} \right|$ is called the *Courant* number. Since the Lax-Wendroff scheme is increasingly accurate as the Courant number approaches to 1, the time and space steps should be chosen so that:

$$\frac{\Delta t}{\Delta x} \text{ is slightly smaller than } \frac{1}{\sup_{x \in [0, L]} v(x)} .$$

2.4. The 2D Menon Model (MM2D). The section is based on [24]. The *2D Menon Model* (MM2D) first partitions the airspace into sectors called *Control Volumes* (CVs) or *Surface Elements* (SEs). These SEs are formed by equal increments in latitudes and longitudes. To simplify the analysis, all the SEs are treated as equal squares. Each SE is then partitioned into eight streams which discretize the notion of directions within a SE (Figure 2). Conceptually, a ninth stream will constitute the input/output of a SE from an underlying airport or from altitudes above or below the desired range of study. Each SE will have three, five or eight entry/exit points with its neighboring SEs depending on its location (corner, border or center), in addition to an eventual airport beneath it.

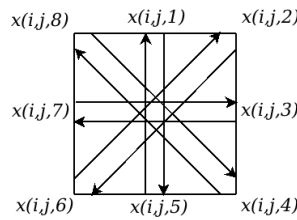


FIGURE 2. Traffic flow directions in an SEL (i, j) . Source: [24].

The MM2D discretizes the time into steps of increments τ . In each time step, a number of aircraft exit from the streams of each SEL. The flow divergence parameter β is a five-dimensional variable. It is time dependent, and determines the percentage of aircraft that switched from streams m to n in the SEL (i, j) . The inertia parameter a is four-dimensional. It characterizes the proportion of aircraft that will stay in a certain stream s of a SEL (i, j) in from time k to $k + 1$. The dynamics of the model can be represented as follows:

$$x_{(i,j,1)}(k+1) = a_{(i,j,1)} \sum_{m=1}^8 \beta_{(i,j,1,m)} x_{(i,j,m)}(k) + \tau y_{(i-1,j,1)}(k) + \tau q_{(i,j,1)}^{\text{depart}}(k) \quad (16)$$

where $x_{(i,j,1)}(k+1)$ represents the predicted number of aircraft in the stream 1 of SEL (i, j) at time step $k+1$; $a_{(i,j,1)}(k)$ represents the fraction of aircraft that will stay in stream 1 of SEL (i, j) after time step k ; $\beta_{(i,j,1,m)}(k)$ represents the portion of aircraft that switched from streams 1 to stream m at time step k before leaving SEL (i, j) at time step $k+1$; $y_{(i-1,j,1)}(k)$ represents the flow at time step k of aircraft into stream 1 of SEL (i, j) , coming from SEL $(i-1, j)$; $q_{(i,j,1)}^{\text{depart}}(k)$ represents the flow at time step k of aircraft into stream 1 of SEL (i, j) coming from an airport located beneath it.

The dynamics of other streams in the SEL can be expressed in a similar way, simply by replacing the number 1 in the index by other numbers (2, 3, \dots , 8). The output flow y is computed as follows:

$$y_{(i,j,m)}(k) = (1 - a_{(i,j,m)}) \sum_{n=1}^8 \beta_{(i,j,m,n)} x_{(i,j,n)}(k).$$

The implementation of the MM2D relies on a two-dimensional geometric partition of the airspace, which is different from the other three models described in

the previous sections. The original work of the authors of the MM2D [24] did not mention how to identify the parameters (a and β in equation (16) of the model). We use one year of ASDI/ETMS data for this identification as follows: from the recorded data, we compute a and β for each day in a full year of data, and take the mean of the a 's and the normalized (by the rule of conservation of flows) mean of the β 's as the parameters a and β respectively.

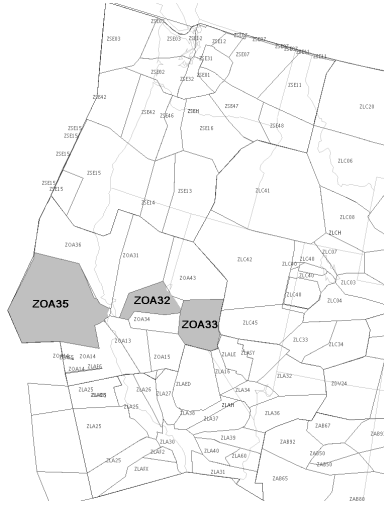


FIGURE 3. Map of the portion of airspace considered in this study: the Oakland ARTCC (ZOA), Los Angeles ARTCC (ZLA), Salt Lake City ARTCC (ZLC), Seattle ARTCC (ZSE), a portion of Denver ARTCC (ZDV), a portion of Albuquerque ARTCC (ZAB), and a portion of Oakland Oceanic ARTCC. Map obtained using the software FACET [5].

2.5. A benchmark scenario for comparison of the models. For the comparison, three of the four models described above (MMM, the CTM(L) and the PDE model) are implemented on the same aggregate traffic flow graph model depicted in Figure 5. The construction of the graph is outlined in the article [34]. The MM2D must be implemented on its own flow structure, because of the two-dimensional nature of the model. The portion of airspace studied for this article is depicted in Figure 3, and consists of 75 sectors of the Oakland, Los Angeles, Seattle and Salt Lake City, Denver, Albuquerque, and Oakland Oceanic Centers. The graph identification procedure relies on the notion of a *path*, illustrated in Figure 4. We use a full year of ASDI/ETMS data for this identification. A portion of the resulting graph is shown in Figure 5. For the MMM, we will use β splits at the nodes where traffic is diverging, following the procedure outlined in the original article [23] and modified according to Section 2.2. For the two other models, we will use the notion of paths, linking any origin to any destination in the graph. This idea is sometimes referred to as the *colored flow paradigm*, which is an example of *multicommodity flows* in the network flow and combinatorial optimization literature [1]. This enables us to avoid the identification of the β split parameters, and the resulting inaccuracies of this model, and most importantly, this uses the fact that the destinations of the aircraft are *known* before take off.

Using the terminology presented before and illustrated in Figure 4, the graph used for this study has 648 paths, 437 links, 12574 cells (MMM), 39776 cells (CTM(L)), and 128500 grid points (PDE model).

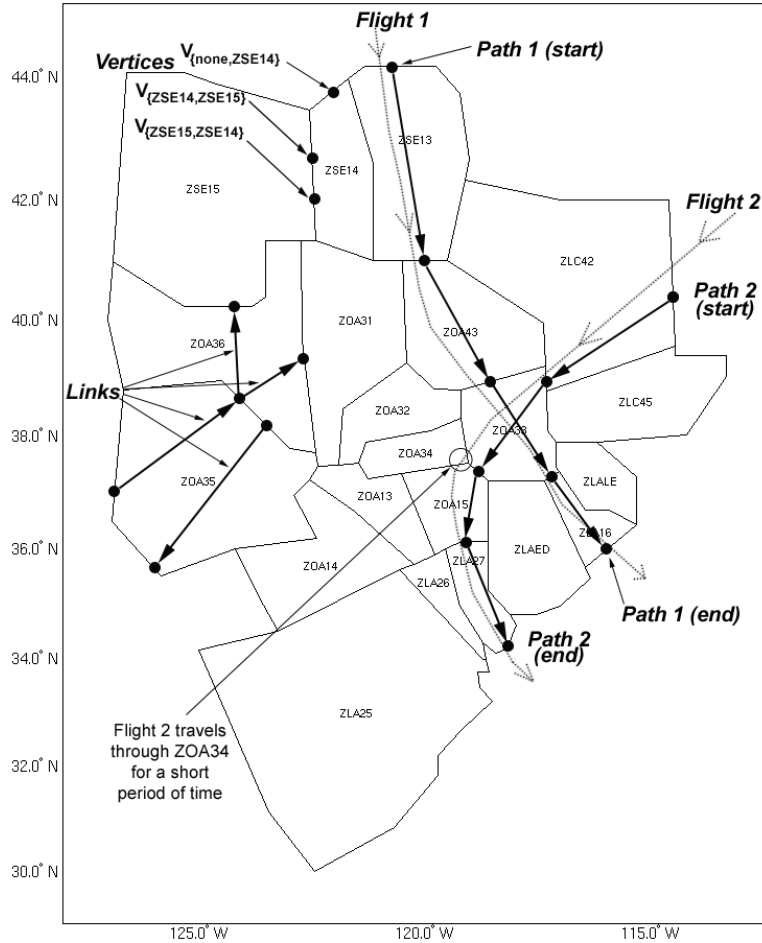


FIGURE 4. Examples of vertices and links for the network flow construction; trajectories and paths.

The parameter identification used for the MMM is straightforward: following the work in [23], we average all velocities of all aircraft over one year for the airspace of interest. For the CTM(L) and the PDE model, we do it path by path. An example of velocity fit for one path is shown in Figure 6. The β split coefficients used for the MMM are computed by dividing the number of aircraft on a branch from a split by the total number of aircraft exiting the split. The cell dimension in the MMM is computed as the distance traveled by an aircraft in one minute (our time step in the simulation). Since the average velocity is 480 knots, this gives a cell dimension of about 15 km. For the CTM(L), the cell dimension is time-based and is one minute in length.

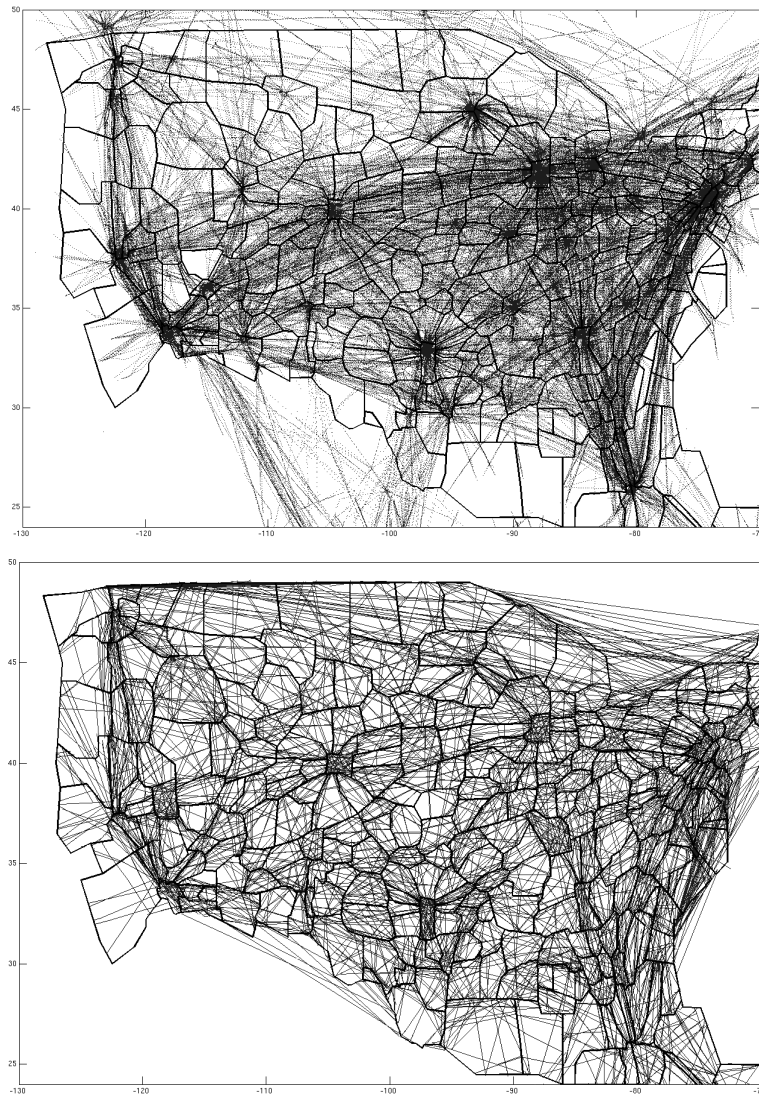


FIGURE 5. **Top:** An example of flight tracks for the full NAS. **Bottom:** Graph model representing the flow patterns above.

3. Model validation. The models are validated against ASDI/ETMS data and their respective performances are compared. The validation procedure consists in taking inputs in the form of filed flight plans (origin-destination and schedule for each aircraft), performing a forward simulation of traffic for the full NAS (with the four models), and comparing the corresponding results with recorded data. The input to each model is the number of aircraft entering the considered region (Figure 3). The predicted states, for example, sector counts, are computed from each model and compared with the recorded data. Simulations are performed from 8:00am GMT on January 24th, 2005 to 8:00am GMT on January 25th, 2005.

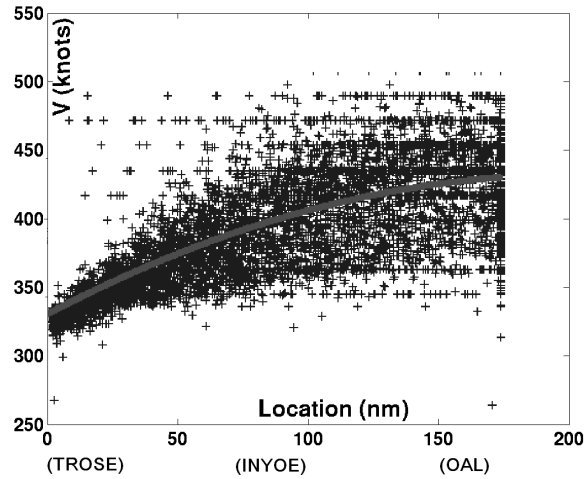


FIGURE 6. Aggregation of velocities along a path. x -axis: positions from the starting point of a path in the model; y -axis: velocities in knots. A third order curve fit is used for the velocity profile. Typically, flights going through this path (passing through waypoints TROSE-INYOE-OAL) pop-up from low altitude airspace and climb up to high altitudes.

Sector counts predicted by the four models are compared with the recorded ASDI/ETMS data. Our study shows that all the sector counts predicted by the four models and ASDI/ETMS data differ from the true counts by noise of a non-negligible magnitude for the following reasons: (1) for the CTM(L), the travel time on a link in the network is computed as the average travel time for all flights in the data set used for the identification; (2) for the PDE model, the velocity profile of each path is filtered from sampled velocities and only several modes are preserved; (3) for the MMM, the split ratios are computed from historical data which usually do not match the instantaneous ratios for a specific day, and also the MMM assumes a uniform velocity across the whole network; (4) for the MM2D, the parameters a and β are computed from historical data, which differ from the actual a and β for a specific day.

A *moving average filter* (MAF) technique is used to filter the sector counts for both the recorded ASDI/ETMS data and the models' simulation data. Applying a MAF to the data requires an appropriate number of data points (time window) in the average. A short time window captures the dynamics of the flow errors but loses the "filtering" benefits, while a long time window filters noise but cancels the error dynamics. To determine a proper size of time window, an experiment involving the maximum sector count error is performed. The maximum count error is the maximum error computed as the absolute difference between the model's sector count and the actual sector count computed from the recorded ASDI/ETMS data, over the course of a simulation. Figure 7 shows the results obtained using different size of time window for the four models in sector ZOA33. The maximum sector count error between filtered ASDI/ETMS data and filtered simulation results of the models decreases when the size of time window increases. In the extreme case,

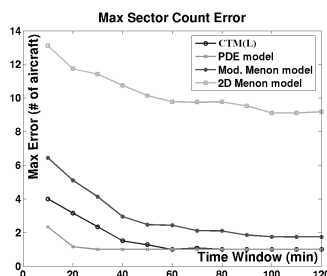


FIGURE 7. Maximum sector count error of ZOA33, between simulation of the models and ASDI/ETMS data (after filtering). The maximum error decreases as the time window increases.

in which the time window is 24 hours (the simulation time span for our study), the error between filtered recorded data and filtered simulation results tends to be zero. This occurs because the error is the difference between the average sector count from ASDI/ETMS data and simulation for a full day, which is very small in general for this case. For example, for the PDE model, the maximum errors are below two when the time window is 20 minutes. Above 20 minutes, increasing the time window does not help significantly to decrease the maximum error, and does not make sense for the problem of interest as well. Removing noise makes physical sense for this problem. Indeed, very often, sector counts exceed legal values for a few minutes (if aircraft are about to exit a sector), which is tolerated in practice, as such flights usually do not pose significant problems to air traffic controllers, and often, hand off procedures for these flights do not occur.

Figure 8 shows the predicted and actual sector counts as a function of time in three sectors: highly loaded sector ZOA33, medium loaded sector ZOA32, and low traffic sector ZOA35. The data shown in the figure is filtered by MAF. From the figures we can see that all the models correctly predict the trends of sector counts.

4. Controller design.

4.1. The Large-capacity Cell Transmission Model. The present section formulates the problem of regulating the aircraft count in different sectors under a legal threshold so that high level TFM actuation can be applied to comply with FAA standards.

The time horizon of the problem (order of magnitude of two hours), is discretized in N time steps of length τ . Therefore, τ is the time spent by one aircraft in one cell in absence of ATC actuation. The state of the system at time step $k \in \{0, \dots, N\}$ is characterized by the number of aircraft in each cell and represented by the vector $x_k \in \mathbb{R}^n$, where n is the number of cells in the network. The control variables are denoted $u_k \in \mathbb{R}^n$ for $k \in \{0, \dots, N\}$, where u_k represents the number of aircraft held in each cell at time step k . The input to the system at time step $k \in \{0, \dots, N\}$ consists of the aircraft entering the network, and the number of aircraft entering each cell at time step k is represented by the vector $f_k \in \mathbb{R}^n$. Note that, unlike in a standard control framework terminology, we do not have control over the input f_k , which is an “exogenous forcing” from outside the system.

Using a standard optimal control framework such as in [6], the dynamics (3)-(4) becomes part of the constraints of the *Mixed Integer Linear Program* (MILP)

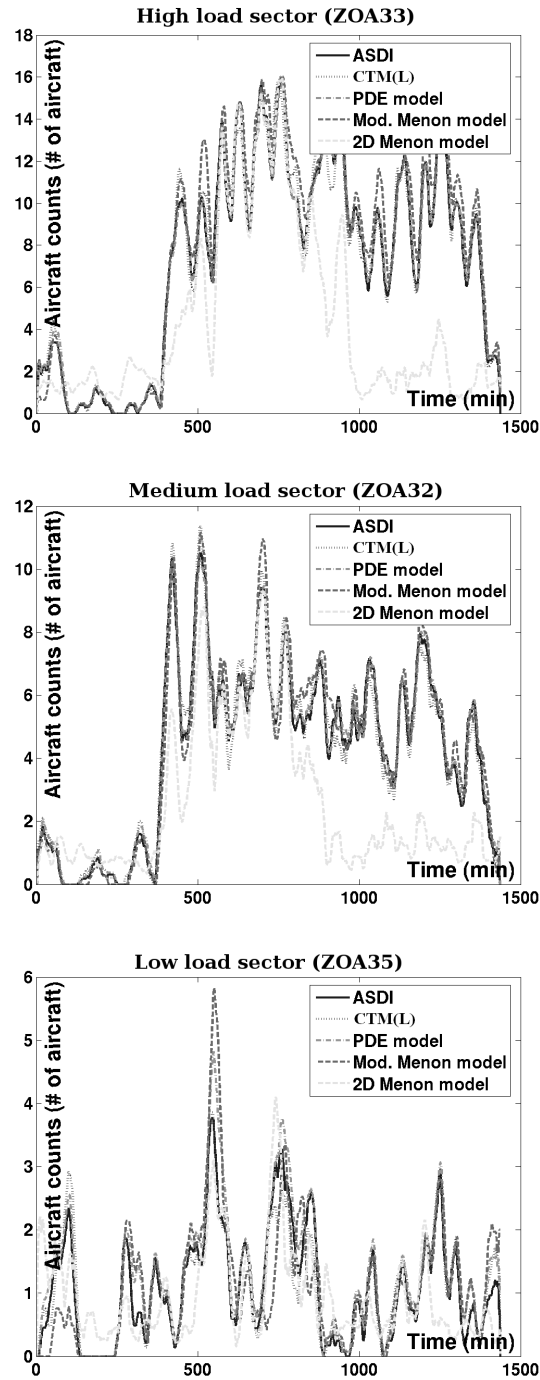


FIGURE 8. Comparison between the predictions of aircraft sector counts predicted by the four models and the actual ASDI/ETMS data counts. Curves represent the processed sector counts after filtering. 0 min corresponds to midnight.

formulation:

$$\begin{aligned}
 \min \quad & \sum_{k=0}^N c^T x_k \\
 \text{s.t.} \quad & E x_k + L u_k \leq M, \quad k \in \{0, \dots, N-1\} \\
 & x_N \in \chi_f \\
 & x_{k+1} = A x_k + B^f f_k + B^u u_k, \quad k \in \{0, \dots, N-1\} \\
 & x_0 = B^f f_0
 \end{aligned} \tag{17}$$

where $\chi_f \subseteq \mathbb{R}^n$ is a terminal polyhedron region, and the matrices E , L , and M represent the constraints on the system: the sector counts must remain under a legal threshold, and the number of aircraft held in a cell cannot be greater than the number of aircraft in that cell. The objective of the problem is to minimize the total travel time; therefore, $c \in \mathbb{R}^n$ is the vector $[\tau, \tau, \dots, \tau]^T$.

4.1.1. *Implementation.* In order to solve (17) in practice, we need to encode it in a computationally efficient manner, which we now present. Flights are clustered on *paths*, as explained in section 3. The set P of paths is determined from the data, as well as the number n_p of cells along path $p \in P$. Within each path, cells are indexed so that flights go through cells of increasing index numbers. The notation for the state of the system, the input and the control variables is adapted to take the paths into account. The state is reindexed, such that $x_{k,p,i}$ now denotes the number of aircraft in cell $i \in \{1, \dots, n_p\}$ of path $p \in P$ at time step $k \in \{0, \dots, N\}$. The corresponding control variables are denoted $u_{k,p,i}$ for $k \in \{0, \dots, N\}$, $p \in P$, and $i \in \{1, \dots, n_p\}$, where $u_{k,p,i}$ represents the number of aircraft held in cell i of path p at time step k . The [forcing] inputs to the system are denoted $f_{k,p}$ for $k \in \{0, \dots, N\}$, and $p \in P$, where $f_{k,p}$ represents the number of aircraft entering the network on path p at time step k .

The sector capacity (i.e. the maximum number of aircraft allowed in the sector) is enforced independently for a set S of different sectors. These sectors, referred to as sector-capacity-constrained sectors, have capacities C_s , $s \in S$. The adapted MILP formulation of the problem is as follows.

$$\begin{aligned}
 \min \quad & \tau \sum_{k=0}^N \sum_{p \in P} \sum_{i=1}^{n_p} x_{k,p,i} \\
 \text{s.t.} \quad & \sum_{(p,i) \in I_s} x_{k,p,i} \leq C_s, \quad k \in \{0, \dots, N\}, s \in S \\
 & 0 \leq u_{k,p,i} \leq x_{k,p,i}, \quad k \in \{0, \dots, N\}, p \in P, i \in \{1, \dots, n_p\} \\
 & x_{k+1,p,i} = x_{k,p,i-1} + u_{k,p,i} - u_{k,p,i-1}, \quad k \in \{0, \dots, N-1\}, p \in P, i \in \{2, \dots, n_p\} \\
 & x_{k,p,1} = f_{k,p} + u_{k,p,1}, \quad k \in \{0, \dots, N\}, p \in P \\
 & x_{0,p,i} = 0, \quad p \in P, i \in \{2, \dots, n_p\} \\
 & x_{k,p,i} \in \mathbb{Z}, \quad k \in \{0, \dots, N\}, p \in P, i \in \{1, \dots, n_p\}
 \end{aligned} \tag{18}$$

where I_s is the set of cells (represented by a path p and a cell number along path p) physically present in sector $s \in S$. The integrality of the number of aircraft in each cell ensures the integrality of the number of aircraft held in each cell, since the input of the system is assumed to be integer.

4.1.2. *LP relaxation of the MILP formulation.* Because problem (18) cannot be solved in polynomial time deterministically, it is relaxed to a *Linear Program* (LP), which is faster to solve in practice, and theoretically polynomial time solvable¹.

The relaxed MILP (i.e. the LP) was solved on a statistical sample of 1,000 different sets of input parameters. 85 percent of the runs lead to an integer solution. For the remaining 15 percent, the optimal solution of the LP (OPT_{LP}) was compared to the optimal solution of the corresponding MILP (OPT_{MILP}). The integrality gap

¹We did not assess the usefulness of the guaranteed computational complexity of LP explicitly in the present case. Indeed, the fact that LPs are polynomial time solvable can only be used with a thorough analysis of the constant multiplying the corresponding higher order monomial.

α , (i.e. $OPT_{MILP} = \alpha \cdot OPT_{LP}$), was always smaller than 1.0015. However, the corresponding solutions are fractional, thus impractical. Several techniques might apply in the future to alleviate this difficulty, in particular LP rounding, which would yield to a suboptimal but integer solution.

On one hand, there is no guarantee of integrality of the LP solution, but on the other hand, the running time of computing the MILPs solution is not guaranteed. Despite the limitations of these two approaches, one conclusion can still be guaranteed from the LP approach: when it returns no solution, it provides a certificate of infeasibility of the corresponding TFM problem with guaranteed running time. Also, given the structure of the problem, minimizing the total travel time is equivalent to minimizing the amount of delay assigned to the aircraft. Therefore, the number of holding patterns provided by the LP solution is the lower bound of the number of holding patterns for which there may exist a physical solution. In other words, no air traffic control actuation can enforce the sector count limitations with less holding patterns than the number of holding patterns provided by the LP relaxation.

4.2. The PDE model. In this section, we study an optimal flow control problem for a network using the PDE model derived earlier. A similar case for highway networks was studied in [12]. We try to mitigate congestion on the network by acting on the coefficients of the allocation matrix. To evaluate the gradient of the objective function, we implement a continuous adjoint method to evaluate its performance. We consider the following problem:

$$\begin{aligned}
 \text{min} \quad & H(m_{ij}) = \sum_{k=1}^{m+n} \int_0^T \int_0^{L_k} \rho_k(x,t) dx dt \\
 \text{s.t.} \quad & \frac{\partial \rho_k(x,t)}{\partial t} + v_k(x) \frac{\partial \rho_k(x,t)}{\partial x} + v'_k(x) \rho_k(x,t) = 0, \quad 1 \leq k \leq m+n, (x,t) \in (0, L_k) \times (0, T) \\
 & \rho_k(x, 0) = \rho_{0,k}(x), \quad x \in [0, L_k] \\
 & \rho_i(0, t) = \frac{q_i(t)}{v_i(0)}, \quad 1 \leq i \leq m, t \in [0, T] \\
 & \rho_j(0, t) = \frac{\sum_{i=1}^m m_{ij}(t) \rho_i(L_i, t) v_i(L_i)}{v_j(0)}, \quad m+1 \leq j \leq m+n, t \in [0, T] \\
 & 0 \leq m_{ij}(t) \leq 1, \quad 1 \leq i \leq m, m+1 \leq j \leq m+n \\
 & \sum_{j=m+1}^{m+n} m_{ij}(t) = 1, \quad 1 \leq i \leq m \\
 & \rho_k(x, t) \leq \rho_k^{\max}, \quad 1 \leq k \leq m+n
 \end{aligned} \tag{19}$$

Minimizing this functional is equivalent to maximizing the outflow of the network; indeed the value of H represents the total amount of time aircraft spend in the network. The control variables are the coefficients of the allocation matrix ($m_{ij}(t)$). This is in fact a case of boundary control since as explained earlier, the density at the left of an outgoing link is directly related to the value of ($m_{ij}(t)$) by:

$$\rho_j(0, t) = \frac{\sum_{i=1}^m m_{ij}(t) \rho_i(L_i, t) v_i(L_i)}{v_j(0)}, \quad m+1 \leq j \leq m+n \text{ and } t \in [0, T]$$

The first two constraints are used to make sure that the model is realistic; all the aircraft have to leave an incoming link and enter an outgoing link. The third constraint implements a maximum density not to be exceeded for each link.

Adjoint methods were first introduced in the late 1980s as a tool for shape optimization, in particular aircraft design [15]. The direct approach which consists in calculating the gradient of the cost functional using finite differences is only possible when the number of control variables is small. In most real life problems, this number is too large making this approach unfeasible. A more efficient way of calculating gradients is to use the adjoint equations and boundary conditions, which can be solved using numerical schemes to yield the gradient of the cost functions.

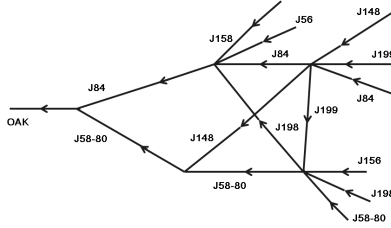


FIGURE 9. Network used for the optimization containing 16 links and 5 junctions. The links are numbered according to the jetways they represent which are part of the ZOA ARTCC.

We will use this technique to determine the gradient of the functional H . We consider links of length L_k , which in our example will be equal to the actual length of the corresponding links of the air traffic network considered. We bring the reader’s attention to the fact that the following results can be applied to any functional

$$H(m_{ij}) = \sum_{k=1}^{m+n} \int_0^T \int_0^{L_k} h_k(\rho_k(x, t)) dx dt$$

for any functions $h_k(x)$. Note that m_{ij} does not appear explicitly in the functional, but implicitly, through the constraints of (19).

4.2.1. *Continuous Adjoint Method.* We will present the continuous adjoint method in this section. We start by forming the variation in the cost function:

$$\begin{aligned} \delta H &= H(m_{ij} + \delta m_{ij}) - H(m_{ij}) \\ &= \sum_{i=1}^m \int_0^{L_i} \int_0^T \rho_i(x, t) dx dt + \sum_{j=m+1}^{m+n} \int_0^{L_j} \int_0^T (\rho_j(x, t) + \delta \rho_j(x, t)) dx dt \\ &\quad - \sum_{i=1}^m \int_0^{L_i} \int_0^T \rho_i(x, t) dx dt - \sum_{j=m+1}^{m+n} \int_0^{L_j} \int_0^T \rho_j(x, t) dx dt \\ &= \sum_{j=m+1}^{m+n} \int_0^{L_j} \int_0^T \delta \rho_j(x, t) dx dt \end{aligned}$$

We then compute the variation of the constraint equation in our case the partial differential equation verified by the density which yields for the outgoing links (the incoming links not being affected by the control):

$$\frac{\partial \delta \rho_j(x, t)}{\partial t} + v_j(x) \frac{\partial \delta \rho_j(x, t)}{\partial x} + v'_j(x) \delta \rho_j(x, t) = 0 \text{ for } m + 1 \leq j \leq m + n$$

with the initial condition:

$$\delta \rho_j(x, 0) = 0$$

and the boundary condition:

$$\delta \rho_j(0, t) = \frac{\sum_{i=1}^m \delta m_{ij}(t) \rho_i(L_i, t) v_i(L_i)}{v_j(0)}$$

Since the variation of the cost function depends on $\delta\rho_j$, we need to add a term to the variation of the cost function to eliminate this dependence; if $\lambda_j(x, t)$ is an arbitrary function, we can add the scalar product of $\lambda_j(x, t)$ with the previous equation since it is equal to zero:

$$\delta H = \delta H + \sum_{j=m+1}^{m+n} \int_0^{L_j} \int_0^T \lambda_j(x, t) \left(\frac{\partial \delta \rho_j(x, t)}{\partial t} + v_j(x) \frac{\partial \delta \rho_j(x, t)}{\partial x} + v'_j(x) \delta \rho_j(x, t) \right) dx dt$$

After integrating by parts:

$$\begin{aligned} \delta H = \delta H + \sum_{j=m+1}^{m+n} \left\{ \int_0^{L_j} \int_0^T \left(-\frac{\partial \lambda_j(x, t)}{\partial t} - \frac{\partial (v_j(x) \lambda_j(x, t))}{\partial x} + v'_j(x) \lambda_j(x, t) \right) \delta \rho_j(x, t) dx dt \right. \\ \left. + \int_0^{L_j} [\lambda_j(x, t) \delta \rho_j(x, t)]_0^T dx + \int_0^T [\delta \rho_j(x, t) v_j(x) \lambda_j(x, t)]_0^{L_j} dt \right\} \end{aligned}$$

Assembling the terms, we obtain:

$$\begin{aligned} \delta H = \sum_{j=m+1}^{m+n} \int_0^{L_j} \int_0^T \left(-\frac{\partial \lambda_j(x, t)}{\partial t} - \frac{\partial (v_j(x) \lambda_j(x, t))}{\partial x} + v'_j(x) \lambda_j(x, t) + 1 \right) \delta \rho_j(x, t) dx dt \\ + \sum_{j=m+1}^{m+n} \left(\int_0^{L_j} [\lambda_j(x, t) \delta \rho_j(x, t)]_0^T dx + \int_0^T [\delta \rho_j(x, t) v_j(x) \lambda_j(x, t)]_0^{L_j} dt \right) \end{aligned}$$

In order to eliminate the dependence of δH on $\delta\rho_j$, we make the following choice for λ_j :

$$\begin{cases} \frac{\partial \lambda_j(x, t)}{\partial t} + v_j(x) \frac{\partial \lambda_j(x, t)}{\partial x} = 1 & m+1 \leq j \leq m+n, (x, t) \in [0, L_j] \times [0, T] \\ \lambda_j(x, T) = 0 & x \in [0, L_j] \\ \lambda_j(L_j, t) = 0 & t \in [0, T] \end{cases} \quad (20)$$

This is the adjoint equation that will be solved to obtain λ_j . Using the boundary and initial conditions for $\delta\rho_j$ and λ_j , we can now compute the gradient of the cost function:

$$\nabla_{m_{ij}} H = - \sum_{j=m+1}^{m+n} \sum_{i=1}^m v_i(L_i) \rho_i(L_i, \cdot) \lambda_j(0, \cdot)$$

At each iteration, we solve the original and adjoint equations using an upwind finite difference scheme and modify the descent direction accordingly using the gradient computed above, which gives the increment in $m_{ij}(\cdot)$. The gradient of the cost functional is used as input in a nonlinear optimization method. A number of nonlinear optimization software are available, for example KNITRO, MINOS, NPSOL, SNOPT, with the first one being used for this article.

The following algorithm was implemented and converged to a minimum of the optimization program:

- 1 Solve the partial differential equations for the density on each link.
- 2 Solve the adjoint equations.
- 3 Evaluate the gradient of the cost functional.
- 4 Use this result in a nonlinear optimisation method.
- 5 Return to step 1 until numerical convergence.

We implement this optimization method on the network represented in Figure 9; the links are taken from the high altitude en route jetways between Salt Lake City

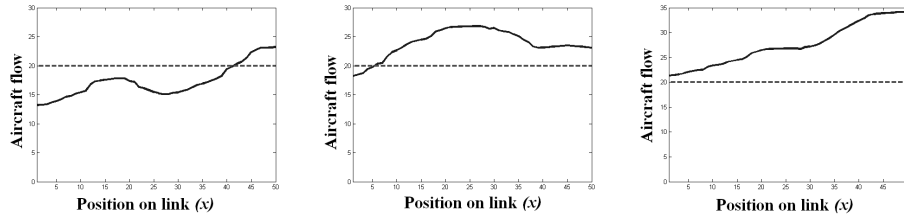


FIGURE 10. Evolution of the aircraft flow in aircraft per hour along the final link at instants $t = 1h$, $t = 2h$, $t = 3h$ in the absence of control; the dotted line represents the threshold flow. As can be seen this limit is exceeded on several occasions.

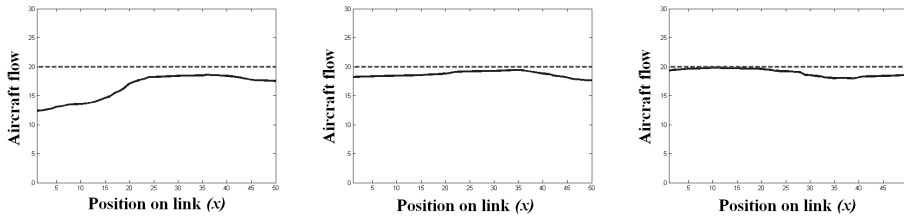


FIGURE 11. Evolution of the aircraft flow in aircraft per hour along the final link at instants $t = 1h$, $t = 2h$, $t = 3h$ with an optimal control strategy. The flow remains below the limit at all times.

and Oakland International Airport. We use jetways J56, J58-80, J84, J148, J156, J158, J198, and J199. The input is constructed using ASDI/ETMS data.

We use the previous method for congestion mitigation, more precisely, we try to keep the aircraft flow on the final approach link to Oakland TRACON under a threshold value of 20 aircraft per hour. We represent the flow at the downstream boundary of the final link at time intervals: 1 hour, 2 hours and 3 hours. The flows in Figure 10 represent the flows without any control being applied, while the flows in Figure 11 are obtained after using the continuous adjoint method. We note that without control, the flows are often above the desirable threshold whereas we manage to maintain the flow under the limit at all times by applying the optimal control strategy. The method used here consists in finding an optimal routing through the coefficients of the allocation matrix that will prevent sudden jumps in aircraft density. These coefficients are automatically adjusted in order to allow the best repartition of aircraft on the network; if a given link is becoming congested, the allocation coefficient that regulates the inflow on this link will decrease and correspondingly the other coefficients at this junction will increase, thus redirecting the aircraft on less congested links. Thus, we are able to maintain a regular spacing between the aircraft even if sudden increases in aircraft density are registered at the entrance of the network. In the absence of control, these jumps in aircraft density are not mitigated and eventually allow the aircraft flow to exceed the limit (Figure 10).

5. Comparison of the four models' performance. When we compare the predictive capabilities of the four models, it can be seen that the four models differ in

accuracy. From the validation performed in Section 3 (see Figure 8 in particular), we can see that the PDE model displays the best prediction capabilities among all the models. As can be seen in Figure 8, the sector count prediction of the PDE model is closer to the recorded ASDI/ETMS data, compared with the other three. In comparing the four models, we will quantify each model's error as well as its computational efficiency.

5.1. Error analysis. The error analysis involves two comparisons: cumulated occurrence of sector count error breach (S), and the instantaneous sector count error. Following the article [29], S is defined as the summation of time intervals under the condition that difference of sector counts between the simulation and ASDI/ETMS data is greater than or equal to a user-specified capacity limitation within a certain time window, which is similar to a cumulative distribution function in statistics. This is summarized in equation (21):

$$S = \sum_{k=1}^T \mathbb{I}_{\{|y_{\text{sim}}^{(k)} - y_{\text{ASDI/ETMS}}^{(k)}| \geq C_s\}} \quad (21)$$

where \mathbb{I} represents the indicator function. The sector count is denoted by $y(k)$, ASDI/ETMS and simulated. The constant C_s is a user-defined threshold. The time window we choose in our simulation is 1440 minutes (24 hours), i.e. $T = 1440$. To measure the similarity in the simulation and the ASDI/ETMS data, different values of C_s are used, and plots of percentage of breaches versus C_s are shown in Figure 12. For example, if we choose $C_s = 3$, the percentage of breaches of the MMM in sector ZOA32 is 15%, which means the predicted sector counts in ZOA32 by the MMM differ from the ASDI/ETMS data by at least three aircraft for 15% of the time. As the value of C_s increases, the breach length for each model tends to zero. This is because C_s is the aircraft count error limit. The PDE model is close to zero breach when the aircraft count error limit is less than five, which has the best predictive performance. The aircraft count error limits which bring the CTM(L) and the MMM to zero breach are higher than the PDE model, while the MM2D requires the largest aircraft count error to bring zero breach.

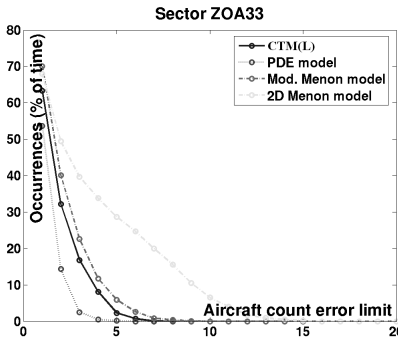


FIGURE 12. Cumulative distribution of breach of sector count error for high load sector ZOA33 (unit is % of the time).

The instantaneous sector count error analysis is performed as well. This error is the difference between the models' aircraft count and the actual aircraft count for each sector computed from the recorded ASDI/ETMS data at each time step in

the simulation. The corresponding relative error is the ratio between the absolute instantaneous error and the actual count. Statistics of the absolute instantaneous error and relative instantaneous error for sector ZOA33 as a function of time for a day are presented in Table 2.

Number	1	2	3	4	5
Name	ZOA13	ZOA14	ZOA15	ZOA31	ZOA32
Number	6	7	8	9	10
Name	ZOA33	ZOA34	ZOA35	ZOA36	ZOA43

TABLE 1. Indices for a portion of the considered sectors in Oakland Center (numbers refer to Figure 13).

Absolute error (aircraft)	Mean	Max	Variance
MMM	1.5456	9	2.4695
MM2D	3.5241	15.8750	12.4788
CTM(L)	1.2373	7	1.7758
PDE	0.7119	5	0.6328
Relative error	Mean	Max	Variance
MMM	0.2706	2.5000	0.0933
MM2D	0.5204	2.3105	0.1579
CTM(L)	0.2000	3	0.0669
PDE	0.1160	2	0.0288

TABLE 2. Instantaneous error (absolute error and relative error) statistics for high load sector ZOA33 on January 1st, 2005.

Figure 13 shows a summary of the max/mean error of the sector counts, and the error variance as well. From Figure 13 we can see that the PDE model exhibits less error and less variance than the other three.

The MM2D model has the largest predictive errors among the four, for two major reasons: (i) The fineness of MM2D depends on the SEL size, a $1^\circ \times 1^\circ$ latitude-longitude tessellation in [24], which is coarse compared with other models. With smaller SEL size, MM2D has more states which increases the computational complexity of the model. (ii) The parameters of MM2D (a and β) are assumed constant, which usually differ from the actual parameters in the time of interest in the real system.

5.2. Computational efficiency. The respective performance of the models are compared (forward simulation). This enables us to assess their computational tractability. For models based on the network graph (the CTM(L), the MMM and the PDE model), it takes approximately 45 minutes to convert the aggregate traffic flow graph model referred to in Section 2.5 according to each model's specifications², while the MM2D model needs approximately three days to identify the system parameters (a and β) using a full year of ASDI/ETMS data. Table 3 lists the CPU time and memory usage for the four models to predict sector counts. The analysis is done for 75 high altitude sectors in Figure 3. The computations are performed on a 1.6 GHz CPU, 2 GB RAM PC running Linux, using the c++ programming language. The CTM(L) has the fastest running time (20 minutes),

²Constructing the graph model alone needs four days, using a full year of ASDI/ETMS data.

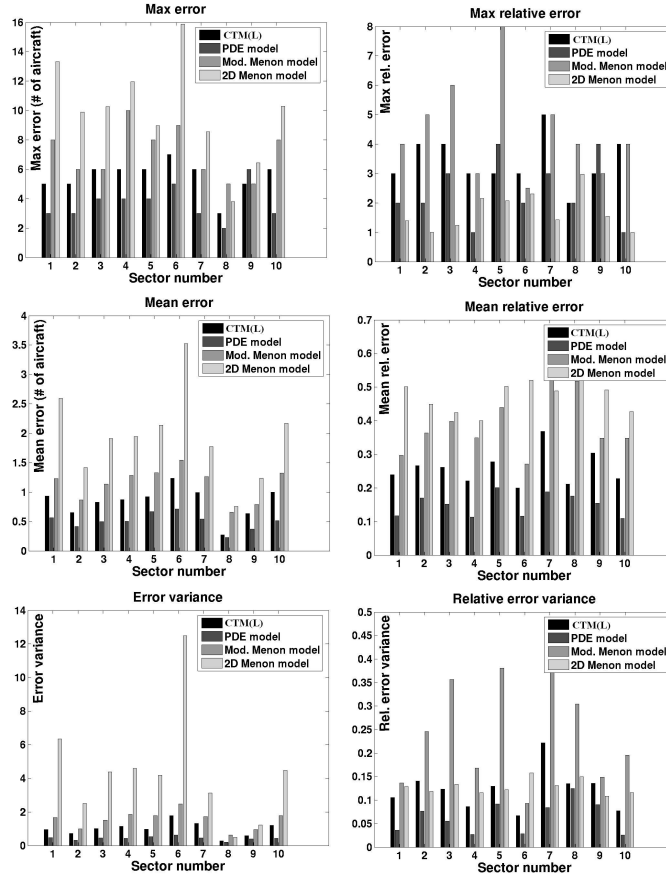


FIGURE 13. **Left:** Summary of the absolute instantaneous error of aircraft sector count. **Right:** The relative error summary. Numbers on the y -axis correspond to the sectors listed in Table 1.

which is about 10 times faster than the PDE model and 15 times faster than the MMM. The running time of the MM2D is relatively faster than the PDE model and the MMM. The difference between the CTM(L) and the PDE model is that the time increments required for a PDE model simulation are smaller than the delay unit used in the CTM(L). The reason why the MMM has the largest running time is because the MMM must keep track of all the merge/diverge nodes in the system, for which a number of matrix multiplications are needed for all merge and diverge nodes at each time step. For the PDE model and the CTM(L), the aircraft count updates are based only on the previous counts and the path length (see Section 2.5). Since the MM2D is based on a different modeling structure, i.e., by partitioning the airspace into small blocks (see Section 2.4; in this study, a $1^\circ \times 1^\circ$ latitude-longitude tessellation is applied), the number of states of the MM2D is smaller than those of the PDE model and the MMM, but larger than that of the CTM(L). This is why the MM2D has comparable computational efficiency to the CTM(L).

6. Conclusion. Four Eulerian models were implemented and compared in our study. We started with the Large-capacity Cell Transmission Model, and then

Models	CTM(L)	PDE	MMM	MM2D
CPU time (minutes)	20	224	310	45
Max RAM usage (MB)	759	1262	697	732

TABLE 3. Computational efficiency (runs performed on a 1.6 GHz CPU, 2 GB RAM PC running Linux, using c++).

presented a modified version of the Menon model adapted to fit a general network topology. We also presented a new application of the Lax Wendroff scheme to a partial differential equation representing air traffic flow. Finally, we implemented the two-dimensional Menon model. The models were applied to high altitude traffic for six Air Route Traffic Control Centers in the National Airspace System. Each model was used for simulation over an entire day. Compared to flight data, the models show accurate predictive capabilities. The models were also compared in terms of their computational time and memory requirements. Control strategies were designed and implemented on similar benchmark scenarios for two of the models, and compared as well.

Future work will include using a full year of Aircraft Situation Display to Industry, Enhanced Traffic Management System data to study hourly/weekly patterns of air traffic flows to show how using these patterns can improve the respective predictive capabilities of each of the models. More simulations, including different days and controlled experiments, will be run in order to underline the strengths and weaknesses of each model. Finally, the models will be used to help designing new features of the Next Generation Air Transportation System. In an ongoing collaboration with Metron Aviation, we will use the Large-capacity Cell Transmission Model to design efficient traffic flow management schemes, in particular, Airspace Flow Programs. The Large-capacity Cell Transmission Model is the most computationally tractable model among the peer models shown in this study. Based on this model, dual decomposition method is currently used for optimization of traffic flows for the full National Airspace System. We will also interface the models with Future ATM Concepts Evaluation Tool to perform automated bottleneck identification, to better understand the effect of weather on traffic flow patterns, in particular, in light of seasonal patterns.

Acknowledgements. This work was initially supported by NASA under Task Order TO.048.0.BS.AF. and later under a NASA NRA NNH06ZNH001 grant (subtopic 4). We are grateful to Dr. Banavar Sridhar for initiating this project, and for his guidance through this work. We are thankful to Dr. Shon Grabbe for his help with ASDI/ETMS data and FACET. We are grateful to Dr. Gano Chatterji for his suggestions regarding the models of the NAS. We want to acknowledge Dr. George Meyer for fruitful conversations on air traffic control and his ongoing support for our research, and to Dr. Charles-Antoine Robelin for his help with generating the initial model, sharing his source code and helping with the graphs presented in this article. We are thankful to Prof. Carlos Daganzo for fruitful discussions on transportation networks. We are grateful to Larry Hogle for helping with the collaboration between UC Berkeley and NASA Ames through the UARC. We are grateful to Dr. Dave Knorr from FAA for his suggestions.

REFERENCES

- [1] R. K. Ahuja, T. L. Magnati and J. B. Orlin, “Network Flows : Theory, Algorithms, and Application,” Prentice Hall, Upper Saddle River, NJ, 1993.
- [2] G. Bastin and V. Guffen, *Congestion control in compartmental network systems*, Systems and Control Letters, **55** (2006), 689–696.
- [3] A. M. Bayen, P. Grieder, G. Meyer and C. J. Tomlin, *Langrangian delay predictive model for sector-based air traffic flow*, AIAA Journal of Guidance, Control and Dynamics, **28** (2005), 1015–1026.
- [4] A. M. Bayen, R. L. Raffard and C. J. Tomlin, *Adjoint-based control of a new Eulerian network model of air traffic flow*, IEEE Transactions on Control Systems Technology, **14** (2006), 804–818.
- [5] K. Bilimoria, B. Sridhar, G. Chatterji, K. Sheth and S. Grabbe, *FACET: Future ATM concepts evaluation tool*, In “Proceedings of the 3rd USA/Europe ATM 2001 R&D Seminar”, Naples, Italy, 2001.
- [6] F. Borelli, “Constrained Optimal Control of Linear and Hybrid Systems,” **290** of *Lecture Notes in Control and Information Sciences*, Springer Verlag, New York, NY, 2003.
- [7] J. M. Coron, B. d’Andréa-Novel and G. Bastin, *A strict Lyapunov function for boundary control of hyperbolic systems of conservation laws*, IEEE Transactions on Automatic Control, **52** (2007) 2–11.
- [8] C. Daganzo, *The cell transmission model: a dynamic representation of highway traffic consistent with the hydrodynamic theory*, Transportation Research, **28B** (1994), 269–287.
- [9] C. Daganzo, *The cell transmission model, part II: network traffic*, Transportation Research, **29B** (1995), 79–93.
- [10] S. Devasia, M. Heymann and G. Meyer, *Automation procedures for air traffic management: A token-based approach*, In “Proceedings of the American Control Conference”, 736–741, Anchorage, AK, May 2002.
- [11] M. Garavello and B. Piccoli, “Traffic Flow on Networks,” **1** of American Institute of Mathematical Sciences on Applied Math, 2006.
- [12] M. Gugat, M. Herty, A. Klar and G. Leugering, *Optimal control for traffic flow networks*, Journal of Optimization Theory and Applications, **126** (2005), 589–616.
- [13] B. Haut and G. Bastin, *A second order model of road junctions in fluid models of traffic networks*, Networks and Heterogeneous Media, **2** (2007), 227–253.
- [14] D. Iamratanakul, G. Meyer, G. Chatterji and S. Devasia, *Quantification of airspace sector capacity using decentralized conflict resolution procedures*, In “Proceedings of the 43rd IEEE Conference on Decision and Control”, 2003–2009, Atlantis, Paradise Island, Bahamas, 2004.
- [15] A. Jameson, *Aerodynamic design via control theory*, Journal of Scientific Computing, **3** (1988), 233–260.
- [16] C. Kirchner, M. Herty, S. Göttlich and A. Klar, *Optimal control for continuous supply network models*, Networks and Heterogeneous Media, **1** (2006), 675–688.
- [17] O. Koroleva, M. Krstic and G. Schmid-Schonbein, *Decentralized and adaptive control of non-linear fluid flow networks*, International Journal of Control, **16** (2006), 801–818.
- [18] S. Larsson and V. Thomee, “Partial Differential Equations with Numerical Methods,” Springer, Berlin, New York, 2003.
- [19] R. J. LeVeque, “Finite Volume Methods for Hyperbolic Problems,” Cambridge University Press, Cambridge, U.K., 2002.
- [20] M. J. Lighthill and G. B. Whitham, *On kinematic waves. II, A theory of traffic flow on long crowded roads*, in “Proceedings of the Royal Society of London”, **229** (1956), 317–345.
- [21] X. Litrico and V. Fromion, *Frequency modeling of open-channel flow*, Journal of Hydraulic Engineering, **130** (2004), 806–815.
- [22] P. O. Malaterre, *PILOTE: Linear quadratic optimal controller for irrigation canals*, Journal of Irrigation and Drainage Engineering, **124** (1998), 187–194.
- [23] P. K. Menon, G. D. Sweriduk and K. Bilimoria, *New approach for modeling, analysis and control of air traffic flow*, AIAA Journal of Guidance, Control and Dynamics, **27** (2004), 737–744.
- [24] P. K. Menon, G. D. Sweriduk, T. Lam, G. M. Diaz and K. Bilimoria, *Computer-aided Eulerian air traffic flow modeling and predictive control*, AIAA Journal of Guidance, Control and Dynamics, **29** (2006), 12–19.

- [25] M. S. Nolan, "Fundamentals of Air Traffic Control," Brooks Cole, Reading, MA, 4th edition, 2003.
- [26] R. L. Raffard, S. L. Waslander, A. M. Bayen and C. J. Tomlin, *A cooperative, distributed approach to multi-agent Eulerian network control: Application to air traffic management*, In "Proceedings of the AIAA Guidance, Navigation and Control Conference and Exhibit", San Francisco, CA, 2005, AIAA Paper 2005-6050.
- [27] P. I. Richards, *Shock waves on the highway*, Operations Research, **4** (1956), 42–51.
- [28] C. Robelin, D. Sun, G. Wu and A. M. Bayen, *En-route air traffic modeling and strategic flow management using Mixed Integer Linear Programming*, In "INFORMS Annual Meeting 2005", New Orleans / San Francisco, 2006.
- [29] C. Robelin, D. Sun, G. Wu and A. M. Bayen, *MILP control of aggregate Eulerian network airspace models*, In "Proceedings of the American Control Conference", 5257–5262, Minneapolis, MN, 2006.
- [30] S. Roy, B. Sridhar and G. C. Verghese, *An aggregate dynamic stochastic model for air traffic control*, In "Proceedings of the 5th USA/Europe ATM 2003 R&D Seminar", Budapest, Hungary, 2003.
- [31] B. Sridhar, T. Soni, K. Sheth and G. Chatterji, *An aggregate flow model for air traffic management*, In "AIAA Conference on Guidance, Navigation, and Control", Providence, RI, 2004, AIAA Paper 2004–5316.
- [32] B. Sridhar, T. Soni, K. Sheth and G. Chatterji, *Aggregate flow model for air-traffic management*, AIAA Journal of Guidance, Control and Dynamics, **29** (2006), 992–997.
- [33] I. S. Strub and A. M. Bayen, *Weak formulation of boundary conditions for scalar conservation laws: an application to highway modeling*, International Journal of Robust and Nonlinear Control, **16** (2006), 734–748.
- [34] D. Sun and A. M. Bayen, *A New Eulerian-Lagrangian Large-capacity Cell Transmission Model for En Route Traffic*, Under review, AIAA Journal of Guidance, Control and Dynamics, 2007.

Received June 2007; revised September 2007.

E-mail address: `sundf@berkeley.edu`

E-mail address: `strub@ce.berkeley.edu`

E-mail address: `bayen@berkeley.edu`